Design of a low-thrust assisted trajectory to Saturn

Elena Fantino[*][†] *and Roberto Flores*[◇] *and Jesús Peláez*[♯]
[*] Khalifa University of Science and Technology
Department of Aerospace Engineering, P.O. Box 127788, Abu Dhabi (United Arab Emirates)
◇ International Center for Numerical Methods in Engineering, Campus Norte UPC, Gran Capitán s/n,
Barcelona (Spain)
♯ Space Dynamics Group, School of Aeronautical and Space Engineering, Technical University of Madrid,
Plaza Cardenal Cisneros 3, Madrid (Spain)
elena.fantino@ku.ac.ae · rflores@cimne.upc.edu · j.pelaez@upm.es
[†]Corresponding author

Abstract

We present the design of a low-thrust trajectory to Saturn with a gravity assist at Jupiter. In the Earth-to-Jupiter portion of the transfer, the propulsion system applies constant thrust in the direction of the orbital velocity to increase the semimajor axis at the fastest rate. After the swingby, the thruster is fired during a portion of the Jupiter-to-Saturn transfer and implements a steering law that minimizes the velocity relative to Saturn at arrival, thus facilitating the orbit insertion.

1. Introduction

The exploration of the outer planets has been prioritized by NASA and ESA: important missions to the Jupiter system (NASA's Europa Clipper, Phillips & Pappalardo,[15] and ESA's Jupiter Icy Moons Explorer, Grasset et al.[12]) are being designed, and studies are underway to launch a follow-up of Cassini/Huygens called Titan Saturn System Mission, a joint ESA-NASA project (Coustenis et al.[8]). However, the design of orbiter missions to the giant planets must face one major challenge: the amount of propellant required for orbit insertion is very high. For Cassini/Huygens the hyperbolic excess speed relative to Saturn at arrival had a magnitude of 5.6 km/s. As a result, the orbit insertion (OI) maneuver had a cost of 622 m/s or 800 kg of propellant. Another 314 kg where consumed for the subsequent pericenter raising (Goodson et al.,[11] Leeds, Eberhardt and Berry[14]). We present a method to minimize the hyperbolic excess speed upon arrival at Saturn, thus reducing the cost of the OI manoeuver. The transfer from Earth to Saturn is assisted with electric propulsion. During the Earth-to-Jupiter transfer, the thruster imparts a constant tangential acceleration to maximize the increase in the orbital energy, allowing a moderate departure C_3 of 67.25 (km/s)^2 which reduces mission costs. The gravity assist (GA) with Jupiter is unpowered and modelled with the patched-conics method. Upon leaving the planet, the thruster is reactivated, this time to reduce the hyperbolic excess speed at Saturn. The guidance strategy in the Jupiter-to-Saturn transfer is treated as a minimization problem. using the hyperbolic excess velocity as error indicator. Its derivatives with respect to the orbital elements are then computed. The rates of change of the orbital elements, as functions of the thrust components, are obtained from Gauss' planetary equations. Using the chain rule yields the rate of change of the error as a function of the thrust vector. The thrust orientation giving the fastest instantaneous decrease of the hyperbolic excess velocity is used, giving a locally-optimum trajectory. When the hyperbolic excess velocity reaches a preset level, the thruster is powered down and the spacecraft coasts to Saturn. In this work, planetary orbits are assumed circular and coplanar, with the trajectory contained in the same plane. Outside of the spheres of influence of the planets, the trajectory is computed with the Sun-spacecraft two-body model, adding the acceleraton due to the propulsion system. The motor characteristics are those of the NASA Evolutionary Xenon Thruster (NEXT), as described by Herman.[13] The selection of the thruster performance parameters is presented in Sect. 2. Section 3 illustrates the design of the Earth-to-Jupiter portion of the trajectory. The design of the GA is dealt with in Sect. 4. Section 5 presents the control law algorithm, whereas the application to the Jupiter-to-Saturn transfer is illustrated in Sect. 6. The results, including the analysis of the optimal transfer and a discussion on the technological feasibility, are exposed in Sect. 7. Conclusions are drawn in Sect. 8. A preliminary version of this work was presented at the 29th AAS/AIAA Space Flight Mechanics Meeting (Fantino et al.[9]).

2. Thruster performance parameters

We assume that the NEXT thruster imparts a constant acceleration of $2.5 \cdot 10^{-5}$ m/s^2, which corresponds to a force of 25 mN on a mass of 1000 kg. This requires an input power of 600 W, with a specific impulse is 1400 s and a propellant flow rate is $1.85 \cdot 10^{-6}$ kg/s. At this flow rate the expected lifetime of the motor is close to 8 years (van Noord[19]).

3. The low-thrust transfer to Jupiter

The minimum-energy direct transfer from Earth to Jupiter is a Hohmann maneuver, requiring a launch C_3 of 77 (km/s)^2 (see Biesbroek[5]). This high energy requires limits the mass injected, even with the most powerful launchers: a Delta IV Heavy (4050H) can only accelerate a 1500 kg payload at this C_3 level (Benson, Riehl & Oleson[3]). A reduced initial specific energy enables the use of lighter launchers for a given spacecraft mass or, alternatively, increase the payload.

In this contribution, we improve the results of a previous study which used a ballistic trajectory to Jupiter (Fantino et al.[9]). We assume that the electric thruster is fired continuously after launch, raising the aphelion of the initial heliocentric orbit in order to reach Jupiter. Thrust is applied in the direction of motion yielding the fastest increase of specific orbital energy.

A double loop on the departure C_3 and the initial flight path angle γ generates the Earth-to-Jupiter trajectories. The range of values for C_3 is between 65 and 72 (km/s)^2 in 0.25 (km/s)^2 increments, whereas γ is made to vary from -15 to +15 degrees in 1 degree steps. For C_3 below 67.25 (km/s)^2, the transfer to Jupiter takes more than seven years (long transfer) because the trajectory does not intersect Jupiter's orbit during the first revolution. If C_3 is above 67.25 (km/s)^2, Jupiter can be reached in less than three years (short transfers). Only short trajectories are retained for further study.

The range of values of the initial flight path angle for which the short transfer is possible is shown on the left plot of Fig. 1. The right graph gives the corresponding Earth-to-Jupiter transfer times. For each value of C_3, the minimum time is obtained for $\gamma=0$ (departure tangent to Earth's orbit which maximizes the initial mechanical energy). The minimum transfer time drops from 2.77 to 2.09 years when C_3 increases from 67.25 to 72 (km/s)^2. This is equivalent to a reduction in propellant consumption from 158 to 119 kg. However, for a typical heavy launcher, the reduction in injected mass due to increased C_3 completely negates this benefit. Therefore it is advantageous to use the minimum C_3, as the payload gain is much larger than the increase in propellant budget. Under these conditions, the compatible γ values are very small.

4. The gravity assist with Jupiter

Jupiter's GA is modeled with the patched conics method. When the spacecraft crosses the orbit of Jupiter, the planet's velocity $\mathbf{V}_J$ is subtracted from the spacecraft velocity $\mathbf{V}_{S/C}^-$. The resulting entry hyperbolic excess velocity $\mathbf{v}_\infty^-$ and the choice of perijove radius r_π determine the Jupiter-centered hyperbola completely, in particular the relative velocity $\mathbf{v}_\infty^+$ at sphere of influence departure and the new heliocentric velocity $\mathbf{V}_{S/C}^+$. For each arrival trajectory, we tested a range of flyby depths from 0.5 to $9.5 \cdot 10^6$ km in increments of $0.5 \cdot 10^6$ km. The post-GA state is the initial condition for the trajectory optimizer.

5. The low-thrust optimal control law

The state vector $\mathbf{s}$ of the spacecraft in Cartesian coordinates is indicated as

$$\mathbf{s}(t) = \begin{bmatrix} \mathbf{r} \\ \dot{\mathbf{r}} \end{bmatrix} = \begin{bmatrix} x \\ y \\ v_x \\ v_y \end{bmatrix}, \tag{1}$$

whereas polar coordinates $\{r, \theta\}$ are defined as follows:

$$\mathbf{r} = r\mathbf{u}_r \;\; ; \;\; \mathbf{u}_r = \begin{bmatrix} \cos\theta \\ \sin\theta \end{bmatrix} \;\; ; \;\; \mathbf{u}_\theta = \begin{bmatrix} -\sin\theta \\ \cos\theta \end{bmatrix}. \tag{2}$$

The specific thrust (i.e., acceleration) $\mathbf{f}$ imparted by the propulsion system is.

$$\mathbf{f}(t) = f_r\mathbf{u}_r + f_\theta\mathbf{u}_\theta. \tag{3}$$

The trajectory of the spacecraft under the combined effect of the gravitational field of the Sun (gravitational parameter μ) and the thruster is computed from

$$\frac{d\mathbf{s}}{dt} = \begin{bmatrix} v_x \\ v_y \\ a_x \\ a_y \end{bmatrix},$$

(4)

where

$$\mathbf{a} = \left(f_r - \frac{\mu}{r^2}\right)\mathbf{u}_r + f_\theta \mathbf{u}_\theta.$$

(5)

Note that $\| \mathbf{f} \| \leq f_{max}$, i.e., the available thrust is fixed. At each point in time, a vector of osculating Keplerian elements (semimajor axis a, eccentricity e, longitude of the pericenter ω and mean anomaly M_0 at epoch) is defined as

$$\mathbf{o}(\mathbf{s}) = \begin{bmatrix} a \\ e \\ \omega \\ M_0 \end{bmatrix}.$$

(6)

The synodic period of the Jupiter and Saturn is 19.9 years. Hence, a long time may be required for the planets to reach a configuration allowing the spacecraft to actually encounter Saturn. Therefore, the departure window must be considered carefully when designing the trajectory. However, in this preliminary analysis we aim at determining the effectiveness of the guidance strategy. Thus, we have not considered the launch window opportunities and we assume that the error function depends only on the semimajor axis and eccentricity of the heliocentric orbit of the spacecraft, i.e., $\Im(a, e)$. Therefore, in the following, we shall focus on a and e exclusively, but the procedure is applicable to all four elements.

We have designed a guidance strategy that maximizes the instantaneous rate of reduction of an error function $\Im(a, e)$, given an initial state vector $\mathbf{s}(0) = \mathbf{s}_0$ and the differential equations Eq. (4) governing the motion of the spacecraft. The effect of the propulsion system is linear with respect to $\| \mathbf{f} \|$. Therefore, the fastest reduction of $\Im$ requires maximum thrust at all times. The only free parameter is the orientation of the thrust vector (β)

$$\mathbf{f} = f_{\max} \left(\sin\beta \, \mathbf{u}_r + \cos\beta \, \mathbf{u}_\theta\right).$$

(7)

The optimal control law is determined by the conditions

$$\frac{\partial}{\partial\beta}\left[\frac{d\Im(\mathbf{o}(\mathbf{s}))}{dt}\right] = 0 \quad \text{and} \quad \frac{d\Im(\mathbf{o}(\mathbf{s}))}{dt} < 0.$$

(8)

We compute the rate of change of the error using the chain rule:

$$\frac{d\Im(\mathbf{o}(\mathbf{s}))}{dt} = \nabla\Im^T \cdot \frac{d\mathbf{o}}{dt}.$$

(9)

For our particular case, where $\Im(\mathbf{o}) = \Im(a, e)$, the gradient is

$$\nabla\Im = \begin{bmatrix} \frac{\partial\Im}{\partial a} \\ \frac{\partial\Im}{\partial e} \end{bmatrix}.$$

(10)

The rate of change of the orbital elements can be expressed in matrix form as

$$\frac{d\mathbf{o}}{dt} = \begin{bmatrix} \dot{a} \\ \dot{e} \end{bmatrix} = \begin{bmatrix} \frac{\partial\dot{a}}{\partial f_r} & \frac{\partial\dot{a}}{\partial f_\theta} \\ \frac{\partial\dot{e}}{\partial f_r} & \frac{\partial\dot{e}}{\partial f_\theta} \end{bmatrix} \cdot \begin{bmatrix} f_r \\ f_\theta \end{bmatrix} = \mathbf{R} \cdot \mathbf{f}.$$

(11)

The components of matrix $\mathbf{R}$ are computed from Gauss' planetary equations[10]

$$\frac{\partial\dot{a}}{\partial f_r} = c_1 \, e \, \sin\nu,$$

(12)

$$\frac{\partial\dot{a}}{\partial f_\theta} = c_1 \left(1 + e\cos\nu\right),$$

(13)

$$\frac{\partial\dot{e}}{\partial f_r} = c_2 \sin\nu,$$

(14)

$$\frac{\partial\dot{e}}{\partial f_\theta} = c_2 \left(\cos\nu + \cos E\right)$$

(15)

where

$$c_1 = \frac{2ah}{\mu\left(1 - e^2\right)} \; ; c_2 = \frac{h}{\mu}. \tag{16}$$

In the expressions above, ν is the true anomaly, E is the eccentric anomaly and h denotes the specific orbital angular momentum. Taking the derivative of Eq. (7) with respect to β gives

$$\frac{\partial \mathbf{f}}{\partial \beta} = f_{\max} \left[\begin{array}{c} \cos\beta \\ -\sin\beta \end{array} \right]. \tag{17}$$

Combining Eqs. (8), (9), (11) and (17) yields the relationship for the optimal thrust angle:

$$\nabla \Im^T \cdot \mathbf{R} \cdot \frac{\partial \mathbf{f}}{\partial \beta} = 0. \tag{18}$$

Let $\nabla \Im^T \cdot \mathbf{R} = \left[\begin{array}{cc} b_1 & b_2 \end{array} \right] = \mathbf{b}^T$. Vector $\mathbf{b}$ is a function of the current state of the system and does not depend on the thrust setting. Its components can thus be directly computed from the instantaneous state vector. Once $\mathbf{b}$ is known, Eq. (18) can be solved for the thrust angle

$$b_1 \cos\beta - b_2 \sin\beta = 0 \;\; \rightarrow \;\; \beta = \arctan\frac{b_1}{b_2}. \tag{19}$$

Equation (19) gives two distinct values of β spread 180° apart. The correct one is determined from the condition

$$\mathbf{b}^T \cdot \mathbf{f} < 0 \; ; \tag{20}$$

the other value corresponding to the fastest increase of the error.

6. Application of the guidance law to the Jupiter-to-Saturn transfer

After the GA the thruster is powered on, generating a constant acceleration of $2.5 \cdot 10^{-5}$ m/s^2. The thrust direction is continually adjusted using the strategy described in the previous section. The hyperbolic excess velocity upon Saturn arrival is used as the error function, forcing the algorithm to minimize the relative velocity. Once this velocity falls below a preset limit the motor is taken offline. We limited the duration of the post-Jupiter thrust arc to 4 years to keep it within the operational limits of the thruster.

For the sake of simplicity, we use the square of the excess velocity as error function

$$\Im(a, e) = V_{ex}^2 = \|\mathbf{v} - \mathbf{v}_S\|_{r=r_S}^2 \,, \tag{21}$$

where the subindex S denotes values of Saturn's orbit:

$$r_S = 9.537 AU \; ; \;\; \mathbf{v}_S = \sqrt{\frac{\mu}{r_S}} \mathbf{u}_\theta. \tag{22}$$

The square of the velocity of the probe upon intersecting Saturn's orbit is

$$V^2 = \mu \left(\frac{2}{r_S} - \frac{1}{a} \right). \tag{23}$$

Note that Eq. (23) is only physically meaningful if the trajectories of the probe and planet really intersect. For the time being, we shall assume that this is the case. From the conservation of angular momentum, the circumferential velocity at intersection is

$$V_\theta^2 = \frac{\mu a \left(1 - e^2\right)}{r_S^2}. \tag{24}$$

By combining Eqs. (21) - (24), the error function becomes

$$\Im(a, e) = (V_\theta - V_S)^2 + \left(V^2 - V_\theta^2 \right). \tag{25}$$

Substituting the variations of the velocity components yields the gradient of the error function:

$$\delta\Im = \mu \left[\begin{array}{cc} \left(\frac{1}{a^2} - \frac{1-e^2}{r_S^2} \frac{V_S}{V_\theta} \right) & \frac{2ae}{r_S^2} \frac{V_S}{V_\theta} \end{array} \right] \cdot \left[\begin{array}{c} \delta a \\ \delta e \end{array} \right] = \nabla \Im^T \cdot \delta\mathbf{o}. \tag{26}$$

In case the trajectories of the planet and spacecraft do not intersect, Eq. (25) gives nonphysical values (which may even become negative in the most extreme cases). A simple fix is to replace it with

$$\Im(a, e) = (V_\theta - V_S)^2 + \left|V^2 - V_\theta^2\right|. \tag{27}$$

Note that Eq. (27) does not compute the relative velocity if there is no intersection, but a useful error indicator is obtained nonetheless (it decreases as the probe's trajectory tends to the planet's orbit). With this change, the error function gradient for orbits that do not intersect becomes

$$\nabla\Im\big|_{NI} = \mu \begin{bmatrix} \frac{1-e^2}{r_S^2}\left(2 - \frac{V_S}{V_\theta}\right) - \frac{1}{a^2} \\ \frac{2ae}{r_S^2}\left(\frac{V_S}{V_\theta} - 2\right) \end{bmatrix}. \tag{28}$$

Direct use of Eqs. (26) and (28) leads to poor performance of the guidance algorithm. Due to the absolute value in Eq. (27), the gradient of the error function presents a discontinuity when the orbits of the spacecraft and planet are tangent. The sudden change in slope forces the steepest descent algorithm into a zigzag path along the line of discontinuity, degrading the performance. This is a common problem with steepest descent methods which can be mitigated with an inertia term that smooths changes in the direction of motion. In our specific application there is a much more efficient alternative because the correct path to follow when the problem arises can be determined beforehand. It is precisely the curve

$$r_\alpha = a(1 + e) = r_S, \tag{29}$$

that is, the orbital elements of the spacecraft must evolve in a way that keeps the aphelion constant. To this end, once the probe's osculating Keplerian trajectory becomes tangent to Saturn's orbit, the guidance algorithm switches to aphelion hold mode. The thrust direction is chosen such that, at the end of the current time step, the predicted aphelion coincides with the orbit of the planet:

$$r_\alpha + \frac{dr_\alpha}{dt}\Delta t = r_S, \tag{30}$$

where Δt is the time step of the numerical integrator. We can rearrange Eq. (30) as

$$\frac{dr_\alpha}{dt} = \frac{r_S - r_\alpha}{\Delta t} = \bar{r}_\alpha, \tag{31}$$

which expands into

$$\nabla r_\alpha{}^T \cdot \frac{d\mathbf{o}}{dt} = \bar{r}_\alpha \text{ where } \nabla r_\alpha = \begin{bmatrix} 1 + e \\ a \end{bmatrix}. \tag{32}$$

Using Eq. (11)

$$\nabla r_\alpha{}^T \cdot \mathbf{R} \cdot \mathbf{f} = \bar{r}_\alpha. \tag{33}$$

Let $\nabla r_\alpha{}^T \cdot \mathbf{R} = \begin{bmatrix} d_1 & d_2 \end{bmatrix}$. Upon substituting Eq. (7), Eq. (33) becomes

$$d_1 \sin\beta + d_2 \cos\beta = \frac{\bar{r}_\alpha}{f_{max}} = d_3. \tag{34}$$

The solution is

$$\beta = \varphi \pm \arccos\left(\frac{d_3}{l}\right). \tag{35}$$

where

$$l = \sqrt{d_1^2 + d_1^2} \ ; \ \varphi = \arctan\frac{d_1}{d_2}, \tag{36}$$

From the two solutions in Eq. (35), one must choose the value of β that causes the fastest rate of decrease of the excess velocity.

7. Discussion

We present a collection of figures that illustrate the results of the transfer strategy. We set the minimum value of V_{ex} at 1 km/s (because further reductions do not yield appreciable reduction of the OI impulse) and also included an upper limit of 1,3 km/s (to reduce clutter in the charts).

A LOW-THRUST TRAJECTORY TO SATURN

- Figure 2 (left) shows the combinations of C_3 and fly-by depth that fulfill the requirements, i.e., short Earth-to-Jupiter transfer, maximum duration of post-GA thrust arc of 4 years, magnitude of hyperbolic excess velocity at thruster cutoff between 1 and 1,3 km/s. As the departure trajectories studied are almost tangent to Earth's orbit, C_3 and the fly-by depth are the most relevant parameters. Trajectories with a high perijove (above $4.5 \cdot 10^6$ to $6 \cdot 10^6$ km, depending on launch energy) give rise to post-GA ellipses with moderate eccentricity and semimajor axis. These do not intersect Saturn's orbit and a long thrust arc is needed just to reach the destination planet. As the thrust duration is limited, the resulting trajectories fail to reach Saturn, or do so with a large relative velocity. On the other hand, when the minimum distance to Jupiter is small (below $2 \cdot 10^6$ km) the post-GA trajectories stretch much farther that the orbit of Saturn and the relative velocity is very high.

- Figure 2 (right) pictures the hyperbolic excess velocity as a function of the departure energy. It shows that it is possible to achieve the minimum relative velocity even when $C_3 = 67.25$ (km/s)^2. Therefore, the constraint for C_3 is not the excess velocity, but the requirement of a short Earth-to-Jupiter transfer.

- Figure 3 (left) plots the combinations of post-GA thrust arc duration and C_3 that meet the mission requirements. The consumption of propellant is directly proportional to the duration of the thrust arc (assuming constant propellant flow rate). Thus trajectories with minimum length of the powered phase are desirable. All the points on the upper row of the chart (4 years of thrust) correspond to excess velocities higher than 1 km/s (and below 1.3 km/s). The rest of the trajectories have relative velocities of 1 km/s (because the motor has been deactivated before the 4 years limit). The minimum thrust arc duration depends weakly on C_3, and is always quite close to 3.67 years, even for low departure energies. This translates into 209 kg of propellant for the Jupiter-to-Saturn transfer (20% of the assumed initial spacecraft mass). Note that the difference between the best and worst solutions in terms of thrust duration is just 0.33 years, equivalent to less than 19 kg of propellant (under 2% of the initial mass).

- In Fig. 3 (right) the total Jupiter-to-Saturn transfer time, including the thrust arc and the coast phase, is plotted against C_3. There is a moderate reduction (about 1 year) of the transfer time for higher values of C_3, meaning the coast phase is shorter (the duration of the thrust arc is almost constant).

- Figure 4 presents the total duration of the powered phase (including the pre- and post-GA thrust arcs) which determines the total propellant budget. The figure shows that the minimum thrust duration ranges from 6.4 years at the lowest C_3 to 6.1 years for high departure energy. The variation is mostly due to the Earth-to-Jupiter segment. Given the characteristics of the launchers available, it is preferable to reduce the launch energy at the expense of a slight increase in electric propellant consumption.

The most efficient trajectories are obtained using the minimum launch energy. Hence, we will restrict further discussion to solutions with $C_3 = 67.25$ (km/s)^2.

Figure 5 (left) plots the hyperbolic excess velocity as a function of the fly-by depth for different values of the initial flight path angle. It is possible to achieve the minimum relative velocity for depths between 1.5 and 3.5 million kilometers. The total time that the propulsion system remains active is shown in the right plot. All the trajectories that minimize the excess velocity have comparable total thrust duration, ranging from 6.44 to 6.85 years. Their Earth-to-Saturn transfer time varies between 12.3 and 13.1 years (see Figure 6.

7.1 The optimal solution

The optimal solution (minimum propellant budget) corresponds to $\gamma=0$ and $r_\pi = 2,5 \cdot 10^6$ km. The total propellant consumption is 367 kg. This includes 158 kg for reaching Jupiter and 209 kg for reducing the relative velocity at Saturn. The total duration of the transfer is 13 years. The orbital elements immediately after the GA are $a_0=7.02$ ua and $e_0=0.386$. Thus, the initial aphelion is 9.73 ua which is close to the orbital radius of Saturn (the post-GA osculating ellipse is almost tangent to Saturn's orbit). Figure 7 (left) shows the evolution of the semi-major axis, eccentricity, excess velocity and thrust angle against time. To accommodate the variables to the scale of Figure 7, some have been offset or scaled: the semi-major axis has been offset by its value immediately after the encounter with Jupiter (a_0), the eccentricity e has been scaled by a factor of 3, and the hyperbolic excess velocity V_{ex} has been offset by its target value (1 km/s). The complete Earth-Jupiter-Saturn trajectory is displayed in the right subplot.

7.2 Electrical power production

The average solar constant drops to 50.5 W/m^2 at Jupiter and 15.0 W/m^2 at Saturn. Generating 600 W of electric power using solar panels would require a very large array, incompatible with a small spacecraft mass. Radioisotope power

systems (RPSs) are the only viable alternative currently. This technology is mature and has flown on all deep space missions to the outer solar system. The GPHS-RTG, the standard radioisotope thermoelectric generator (RTG) used in all NASA probes, produces 285 W at beginning of life and 255 after 5-10 years of operation with a mass of 55 kg (Bennett, Lombardo & Rock[2]). A set of three units would be able to power the thruster and provide some extra energy for other systems. Moreover, the waste heat from the RTGs can be used to maintain the temperature of the spacecraft without draining the electric system. Upon arrival at Saturn, the generators can be used to drive the scientific payload.

8. Conclusions

This work presents an optimal control law for interplanetary low-thrust transfers. The technique is, in essence, an application of the classical gradient descent optimization method (Cauchy[6]). The resulting steering law is somewhat reminiscent of the Q-guidance method for missile targeting, with the hyperbolic excess velocity taking the place of the velocity-to-be-gained vector (see Battin[1]). When applied to the design of a transfer to Saturn via gravity assist with Jupiter, the technique finds the thrust direction that maximizes the rate of reduction of the hyperbolic excess speed. For the Earth-to-Jupiter segment the acceleration is imparted in the direction of motion to achieve the fastest increase of the orbital. Two major benefits of the strategy are:

1. The minimum launch C_3 is reduced from 77 $(km/s)^2$ (Earth-to-Jupiter Hohmann transfer) to 67.25 $(km/s)^2$. This permits an increase in injected payload of 800 kg based on the characteristics of a typical heavy launcher (Benson, Riehl & Oleson[3]) or, conversely, using a smaller booster for the same payload. The payload increase completely offsets the propellant required by the electric motor, which is just 158 kg.

2. The post-GA thrust arc reduces the hyperbolic excess velocity at Saturn to 1 km/s using 209 kg of propellant. This lowers the orbit insertion impulse to 148 m/s for the same conditions as the Cassini/Huygens mission, which required a ΔV of 622 m/s. The lower impulse opens the door for alternative braking methods, such as electrodynamic tethers (Cosmo & Lorenzini,[7] Sanmartín et al.,[17] Sanmartín, Peláez & Carrera-Calvo[16]), which have potential for large efficiency improvements.

The concept presented paves the way for missions to explore Saturn and its moons with spacecraft masses below one tonne (as opposed to 5600 kg for Cassini/Huygens) using existing electric propulsion technologies. This enables use of smaller launchers, significantly reducing the overall mission cost. Besides, the control-law is robust because it does not rely on a predefined reference path. Given that the only inputs are the current and target states, it can compensate in real time for deviations from to the nominal trajectory (i.e., separate course correction maneuvers are not needed). The algorithm is very general and is not limited to the specific application described here. For example, we applied it to optimum low-thrust transfers between libration points of the Saturn system. The algorithm delivers good performance on commodity CPUs. Computing 10 000 trajectories in a current laptop processor (Core i7-8750H) needs under 1,3 CPU seconds.

9. Acknowledgments

References

[1] R. H. Battin. Space guidance evolution - a personal narrative. *Journal of Guidance*, 5(2):97 – 110, 1982.

[2] G. L. Bennett, J. J. Lombardo, and B. J. Rock. *Power Performance of the General-Purpose Heat Source Radioisotope Thermoelectric Generator*. M. S. El-Genk and M. D. Hoover Eds., Orbit Book Company, Malabar, Florida, 1987.

[3] S. Benson, J. Riehl, and S. Oleson. Next ion propulsion system configurations and performance for Saturn system exploration. In *43rd AIAA/ASME/SAE/ASEE Joint Propulsion Conference and Exhibit*, 2007. 8-11 July, Cincinnati, OH.

[4] M. Seetharama Bhat and Shashi K. Shrivastava. An optimal Q-guidance scheme for satellite launch vehicles. *Journal of Guidance, Control, and Dynamics*, 10(1):53–60, 1987.

[5] R. Biesbroek. *Lunar and Interplanetary Trajectories*, chapter 2, pages 19–39. Springer Praxis Books, Springer, Cham, 2016.

[6] A. Cauchy. Méthode générale pour la résolution des systémes d'équations simultanées. *C. R. Acad. Sci. Paris*, 25:536–538, 1847.

[7] M. L. Cosmo and E. C. Lorenzini. Tethers in Space Handbook. Technical report, NASA Marchall Space Flight Center, 1997.

[8] A. Coustenis, J. Lunine, D. L. Matson, C. Hansen, K. Reh, P. Beauchamp, J.-P. Lebreton, and C. Erd. The Joint NASA-ESA Titan Saturn System Mission (TSSM) Study. In *Lunar and Planetary Science Conference*, volume 40 of *Lunar and Planetary Science Conference*, page 1060, March 2009.

[9] E. Fantino, J. Pelaez, and V. Raposo-Pulido. Gravitational capture at saturn with low-thrust assistance. In *29th AAS/AIAA Space Flight Mechanics Meeting*, 2019. 13-17 January, Maui, HI.

[10] C. F. Gauss. *Exposition d'une nouvelle méthode de calculer les perturbations planétaires avec l'application au calcul numérique des perturbations du mouvement de Pallas (1812)*, volume 7, pages 439–472. Werke. Hrsg. von der Göttingen K. Gesellschaft der Wissenschaften zu Göttingen, 1870.

[11] Troy Goodson, Donald Gray, Yungsun Hahn, and Fernando Peralta. Cassini maneuver experience-launch and early cruise. In *Guidance, Navigation, and Control Conference and Exhibit*, 1998.

[12] Olivier Grasset, M. K. Dougherty, A. Coustenis, E. J. Bunce, C. Erd, D. Titov, M. Blanc, A. Coates, P. Drossart, L. N. Fletcher, et al. JUpiter ICy moons Explorer (JUICE): An ESA mission to orbit Ganymede and to characterise the Jupiter system. *Planetary and Space Science*, 78:1–21, 2013.

[13] Daniel A. Herman. NASA's Evolutionary Xenon Thruster (NEXT) Project Qualification Propellant Throughput Milestone: Performance, Erosion, and Thruster Service Life Prediction After 450 kg. Technical report, Glenn Research Center, Cleveland, Ohio, 2010.

[14] M. W. Leeds, R. N. Eberhardt, and R. L. Berry. Development of the Cassini spacecraft propulsion subsystem. In *32nd AIAA/ASME/SAE/ASEE Joint Propulsion Conference*, 1996. 1-3 July, Lake Buena Vista, FL.

[15] Cynthia B. Phillips and Robert T. Pappalardo. Europa Clipper mission concept: Exploring Jupiter's ocean moon. *Eos, Transactions American Geophysical Union*, 95(20):165–167, 2014.

[16] J. R. Sanmartín, J. Peláez, and I. Carrera-Calvo. Comparative Saturn-versus-Jupiter Tether Operation. *Journal of Geophysical Research: Space Physics*, 123(7):6026–6030, 2018.

[17] Juan R. Sanmartín, Mario Charro, Henry B. Garrett, Gonzalo Sánchez-Arriaga, and Antonio Sánchez-Torres. Analysis of tether-mission concept for multiple flybys of moon Europa. *Journal of Propulsion and Power*, 33:338—342, 2017.

[18] G. Schmidt. The nasa evolutionary xenon thruster (next): The next step for U.S. deep space propulsion. In *59th International Astronautical Congress*, 2008. 29 September - 3 October, Glasgow, UK.

[19] Jonathan Van Noord. Lifetime assessment of the next ion thruster. In *43rd AIAA/ASME/SAE/ASEE Joint Propulsion Conference and Exhibit*, 2007. 8-11 July, Cincinnati, OH.
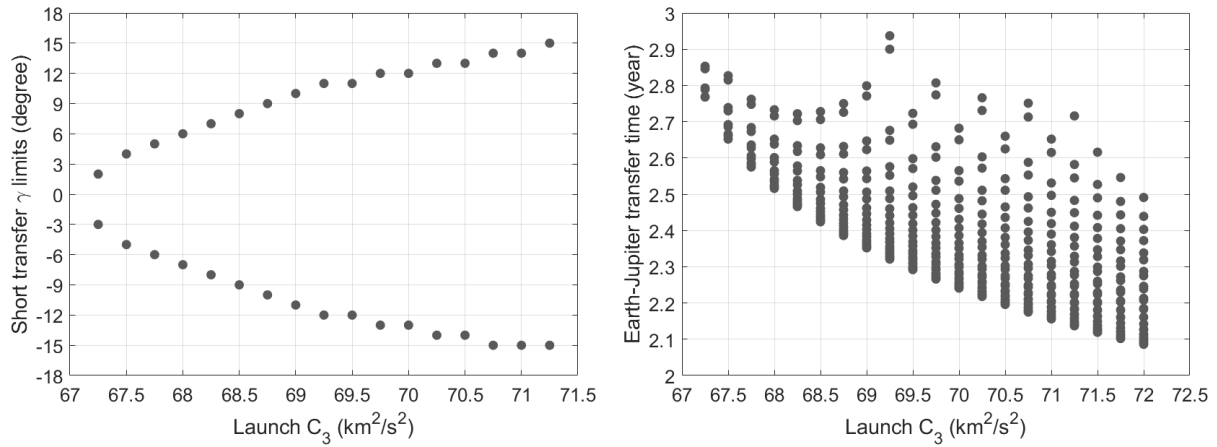
Figure 1: Left: Departure flight path angle limits for short Earth-to-Jupiter transfers. Right: Earth-to-Jupiter transfer time vs. launch C_3 for short transfers.
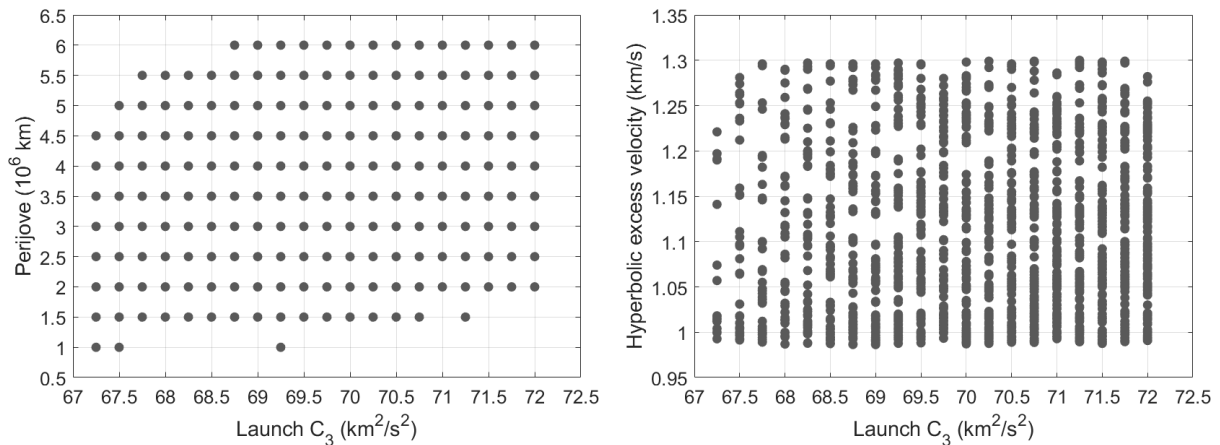
Figure 2: Left: Combinations of launch C_3 and fly-by depth that respect the mission constraints. Right: Saturn V_{ex} vs. launch C_3
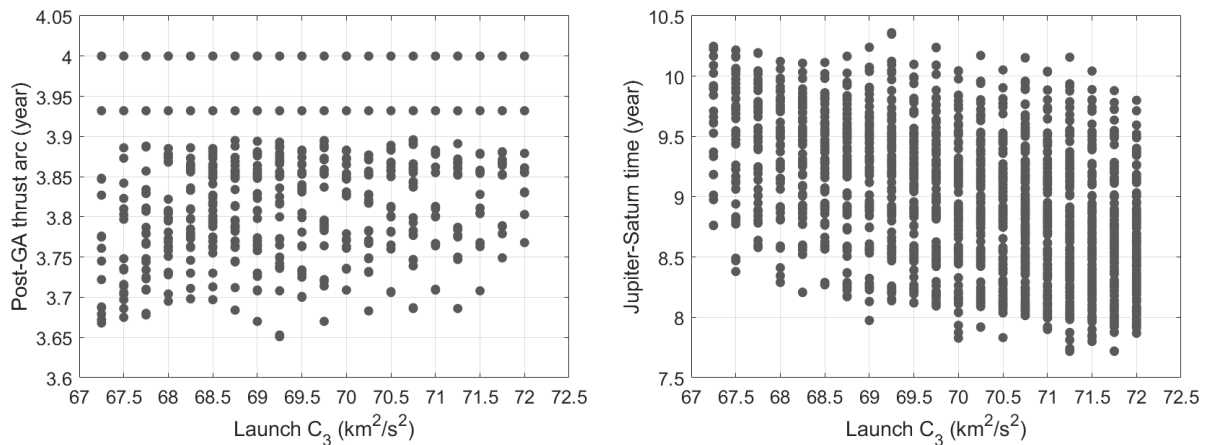
Figure 3: Left: Jupiter-Saturn thrust arc length vs. launch C_3. Right: Jupiter-to-Saturn transfer time vs. launch C_3.

A LOW-THRUST TRAJECTORY TO SATURN
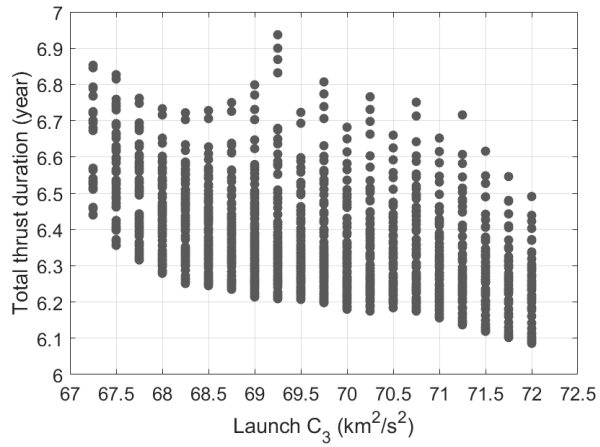
Figure 4: Total length of the powered phase vs. launch C_3.
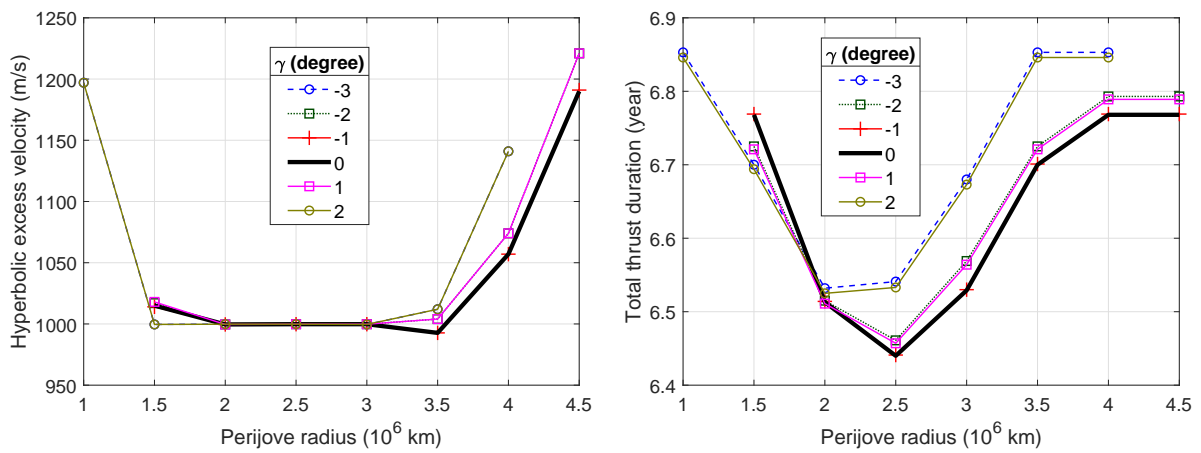
Figure 5: C_3=67.25 (km/s)^2. Left: Saturn V_{ex} vs. GA depth. Right: Total length of the powered phase vs. GA depth.
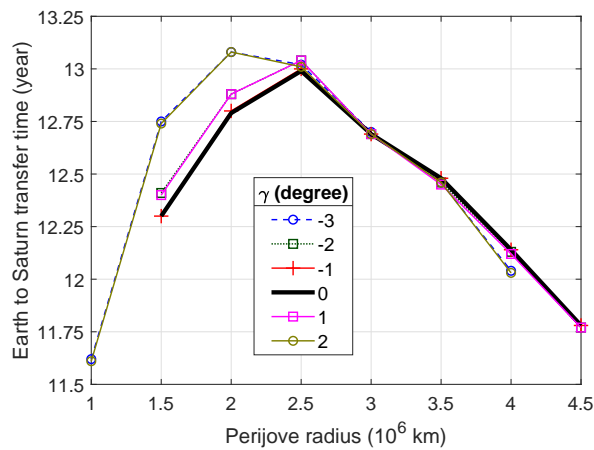
Figure 6: Earth-to-Saturn transfer time vs. GA depth (C_3=67.25 (km/s)^2).
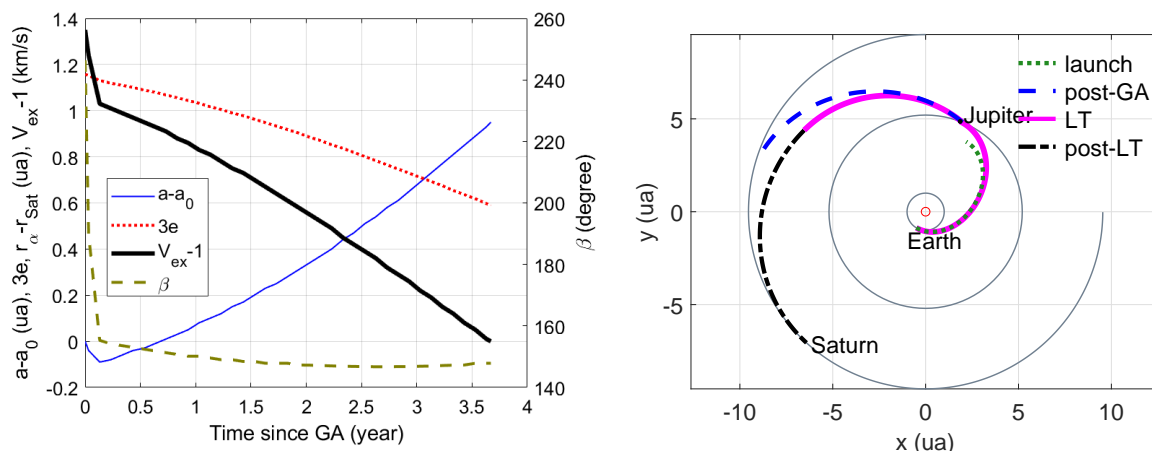
Figure 7: The optimal solution: $\gamma=0$, $r_\pi=2.5 \cdot 10^6$ km, $C_3=67.25$ (km/s)^2. Left: Semi-major axis, eccentricity, hyperbolic excess velocity and thrust angle vs. time after GA. Right: Earth-Jupiter-Saturn trajectory; powered (solid pink) and coast (dot-dashed black) phases; post-launch (dotted green) and post-GA (dashed blue) osculating ellipses.